Formation of oxides in the interior of friction stir welds

Judy Schneider (UAH)
Po Chen (Jacobs ESSSA)
Arthur C. Nunes, Jr. (NASA-MSFC)

1.0 Abstract

In friction stir welding (FSWing) the actual solid state joining takes place between the faying surfaces which form the weld seam. Thus the seam trace is often investigated for clues when the strength of the weld is reduced. Aluminum and its alloys are known to form a native, protective oxide on the surface. If these native surface oxides are not sufficiently broken up during the FSW process, they are reported to remain in the FSW interior and weaken the bond strength. This type of weld defect has been referred to as a lazy "S", lazy "Z", joint line defect, kissing bond, or residual oxide defect. Usually these defects are mitigated by modification of the process parameters, such as increased tool rotation rate, which causes a finer breakup of the native oxide particles.

This study proposes that there may be an alternative mechanism for formation of oxides found within the weld nugget. As the oxidation rate increases at elevated temperatures above 400ºC, it may be possible for enhanced oxidation to occur on the interior surfaces during the FSW process from entrained air entering the seam gap. Normally, FSWs of aluminum alloys are made without a purge gas and it is unknown how process parameters and initial fit up could affect a potential air path into the interior during the processing. In addition, variations in FSW parameters, such as the tool rotation, are known to have a strong influence on the FSW temperature which may affect the oxidation rate if internal surfaces are exposed to entrained air.

A series of FSWs were made in 3 different thickness panels of AA2219 (0.95, 1.27 and 1.56 cm) at 2 different weld pitches. As the thickness of the panels increased, there was an increased tendency for a gap to form in advance of the weld tool. If sufficient air is able to enter the workpiece gap prior to consolidation, the weld temperature can increase the oxidation rate on the interior surfaces. These oxidation rates would also be accelerated in areas of localized liquation. Metallographs from the weld panels showed indications of liquation at the grain boundaries. In FSWs of thicker panels, these regions of liquation were found to be heavily oxidized. The quality of the FSWs was evaluated from tensile testing at room temperature. As the panel thickness increased, a slight decrease in tensile strength was observed which was attributed to the presence of oxides. No oxide formation was observed in the thinner workpieces, although there were indications of localized liquation at the grain boundaries.

Results from this study will assist in a better understand of the mechanisms of oxide formation in FSW interiors and provide methodology for minimizing their occurrence.

2.0 Background

2.1 Aluminum and its alloys

Aluminum alloys are used extensively in the aeronautical and astronautical industries due to their high strength to weight ratio, corrosion resistance, and cryogenic compatibility. Of particular interest is the 2xxx series aluminum alloys which are strengthened by precipitates formed during appropriate heat treatments. By using the solid state joining technique of FSWing, improved properties can be obtained in weldments of these 2xxx series alloys. Although the solid state joining technique eliminates many of the metallurgical issues associated with conventional fusion welding, there continues to be concern regarding the re-deposition of the native oxide present on the faying surface and its subsequent impact on material properties. Because the joining temperatures are below the dissociation temperature of 2054 ºC, the aluminum oxide (Al_2O_3) can only be reduced by mechanical means such as mechanical abrasion or by the shearing action of the FSW process which exposes clean surfaces to be joined.

2.2 Aluminum Oxidation Rate

A film of Al_2O_3 is always present on the surface of aluminum and its alloys. Based on the Pilling-Bedworth Ratio, this oxidation layer is predicted to be protective. Most theories and studies which regard the oxidation of solid aluminum, consider the first monolayer of oxidation to be virtually instantaneous, and only dependent on the arrival rate of oxygen. This monolayer develops into an amorphous layer whose rate of oxidation is dependent upon both the oxygen arrival rate and the rate of diffusion through the existing oxide layer. Earlier studies published the stable oxide layer at thickness of 2-3 nm [1, 2, 3]. Later studies found that the crystalline structure and orientation [4] affected the oxide thickness expanding the range from 0.5 nm [4] to 4 nm [5].

The rate of oxidation for aluminum is reported to be influenced by both temperature and moisture [6]. The kinetics of aluminum oxidation follows a parabolic law in the temperature range 350 to 475 ºC, reaching an equilibrium thickness rapidly. At low temperatures (<300º C) the oxide film growth rate is considered to be very fast initially, followed by an abrupt and drastic reduction to virtually zero, or self-limiting, within less than 250 s [7, 8]. At higher temperatures, the oxidation follows a linear law and can reach a greater thickness [7]. The kinetic rate is further reduced if the initial surface oxide is crystalline rather than amorphous. The native oxide layer is amorphous, but can crystallize at elevated temperatures. Thus oxidation rates at elevated temperatures (> 500º C) are reported to stabilize in thickness at approximately 200 nm [7, 8].

The effect of alloying elements on the oxidation rate for molten aluminum [9] was found to increase with the addition of sodium, lithium, calcium, and magnesium [10, 11]. Effect of alloying elements on the oxidation rate of solid metal has been evaluated for electroplating and anodizing studies in which the Mg content correlated with an increase in oxidation rate [12].

Based on the literature, the concern regarding initial oxidation films on the workpiece would not be expected to be affected by delays between cleaning and FSWing. This stable layer would not be expected to increase as a function of additional time at room temperature. As a stable oxide layer of 1-2 nm is noted to form within 250 s, any further delay in cleaning would not be expected to result in thicker oxide layers. Even in the presence of high humidity, a stable layer is still expected to form within seconds. However the noted change in oxidization rates at temperatures greater than 500 ºC, suggest that the remnant line oxides may come not from the native oxides on the surface of the aluminum workpiece, but occur during the FSW process. Thus the occurrence of joint line remnants may correlate with FSW temperature due to weld parameters as they influence the FSW temperature and resulting weld microstructure [13, 14].

2.3 Joint Line Defects

Various reports have been published in the literature regarding the behavior of the initial oxide layer on the base material surface and its effect on the resulting mechanical properties of FSW aluminum alloys. If these oxides are not adequately dispersed in the FSW, they can remain in the weld nugget and result in a typical "joint line remnant" defect as shown in Figure 1. The joint line remnant typically comprises an array of oxides that can be seen from the macrostructure at very low magnifications. The joint line remnant is also referred to as; kissing bond, lazy S, lazy Z, or residual oxide defect [15, 16, 17, 18, 19].

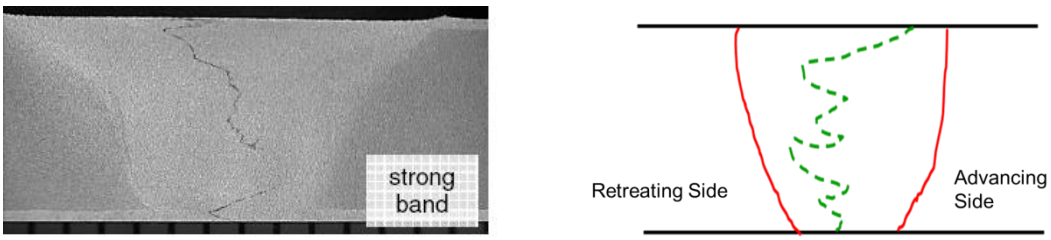

(a) (b)

Figure 1. Metallographic image (a) of a conventional FSW which shows a typical joint line remnant feature and (b) illustration of the pattern [20].

Models of the FSW process have promoted the understanding that the joint is formed as the rotation of the pin surface shears the metal thereby exposing un-oxidized surfaces which bond under the resulting load as the tool advances [21, 22, 23, 24]. The resulting fragmented Al_2O_3 particles flow collectively during the FSW process and, if of sufficient size, may accumulate in the lazy S feature reported. Since the amount of flow increasing varies from the root to the crown in conventional FSW, most remaining oxide particles are reported near the root region [25]. Offsetting the pin to the RS is expected to reduce the size of the oxide to the point of no detection [26] due to the increasing amount of shearing strain.

Krishnan [26] commented on the report of oxides in a manuscript by Larsson [27] and speculated that oxides could form along the layers of metal as they are sheared and consolidated in the wake of an aluminum alloy FSW. Speculation was made that at some point in time, purge gases might be required to avoid oxidation. Since then various studies have investigated the effect of the joint line remnant on mechanical properties and have found no detrimental effect [15, 18, 19,

25]. Only one study found a degradation of properties and that was in tensile testing of AA2219-O that was subjected to a post weld heat treatment. However, from the images presented, the weldment also experienced abnormal grain growth which was not discussed as a contributing factor [19].

In a study by Saito [25], TEM studies of the particles along the remnant line were found to be amorphous Al_2O_3. This indicated that the oxides were not subjected to high temperatures for any length of time. Because of the amorphous nature, the oxides were attributed to native oxide films on the aluminum surfaces prior to the FSW. Findings in a study by Li et al [15] contrast the results of Saito [25] and reported the presence of coarsened particles of precipitated Al_2Cu phase in the region around a kissing bond defect. Thus this study suggested higher temperatures occurred resulting in the coarsening. No information was provided on identification of any oxide phases present.

Most studies indicate that the joint line remnant can be eliminated by proper selection of FSW parameters of tool rotation, travel, and tilt [15, 18, 28, 29, 30, 31]. In many studies, the remnant line was only visible when the workpiece surfaces were anodized prior to the FSW [17, 18]. Thus these studies indicate that the joint line remnant is not an indication of inadequate cleaning or extended delay between pre-weld cleaning and the FSW, but rather an indication of non-optimized FSW parameters.

3.0 Experimental procedure

In this study, self-reacting (SR) FSWs were made in 3 different thicknesses of panels of AA2219-T87 that were nominally 10 cm wide by 61 cm long. Panel thicknesses used were 0.95, 1.27, and 1.59 cm. All welds were made in the butt weld configuration using the LEGIO machine at the NASA-Marshall Space Flight Center operated in load control. A threaded pin with 3 flats was used with a scrolled shoulder. All panels were stitch tacked prior to the SR-FSW process using a conventional FSW tool with a shortened pin.

The weld parameters are summarized in Table I along with the logged torque for the shoulder and the pin. The LEGIO configuration independently drives the upper shoulder from the pin and lower shoulder. Thus there is a separate torque measurement associated with the upper shoulder, and another torque measurement associated with the pin and lower shoulder. Because of the combined drive of the pin and the lower shoulder, the pin/lower shoulder torque has a higher value.

Nominally three specimens were removed from each weld panel and metallographically prepared. The specimens were taken from the beginning section of the weld and designated M01, the middle of the weld and designated M02, and the end of the weld and designated M03. The specimens were mounted in a phenolic, ground, polished, and etched using Keller's to reveal the macrostructure.

Macrographs were made of the etched and polished specimens using a Nikon digital camera with a macro lens. Higher magnification images were made using an environmental, field emission

(FE) FEI Quanta 600 scanning electron microscope (SEM) operated at 8 and 15 keV and configured with an energy dispersive spectrometer (EDS) operated at 15 keV.

A total of 6 specimens were tested at room temperature for each of the 6 panels per material thickness. The tensile tests were conducted in displacement control at a rate of 0.127 mmpm. Stress measurements were calculated using the load cell data and specimen cross sectional area. Strain measurements were obtained directly from the use of extensometers.

Table I. SR-FSW Schedule

Panel ID	Thickness (cm)	Pinch force (kN)	Weld pitch (rev/mm)	Spindle torque (lbs)	Pin torque (lbs)
P13	0.95	0.9	6.40	113	147
P14	0.95	0.9	6.40	107	154
P15	0.95	0.9	6.40	108	154
P16	0.95	0.9	6.73	118	143
P17	0.95	0.9	6.73	125	140
P18	0.95	0.9	6.73	124	137
P01	1.27	2.2	7.31	143	265
P02	1.27	2.2	7.31	143	262
P03	1.27	2.2	7.31	145	260
P04	1.27	2.2	8.44	162	215
P05	1.27	2.2	8.44	163	213
P06	1.27	2.2	8.44	164	215
P07	1.59	2.0	7.87	170	292
P08	1.59	2.0	7.87	161	295
P09	1.59	2.0	7.87	154	301
P10	1.59	2.2	8.72	179	250
P11	1.59	2.2	8.72	162	262
P12	1.59	2.2	8.72	168	259

4.0 Results

4.1 Mechanical Properties

Figures 2, 3, and 4 present the mechanical property data for the 0.95, 1.27, and 1.59 cm panel thickness, respectively. These figures compare the data for high vs low weld pitch for the panels tested at room temperature (RT). With the exception of Figure 4 for the 1.59 cm thick panels, little variation is noted in the mechanical properties at either weld pitch. Representative specimens for metallurgical analysis were selected on the basis of nominal and lowest properties and are summarized in Table II normalized to the acceptance values for the UTS of each thickness panel [32]. Low properties of specimens found within these weld panels are highlighted.

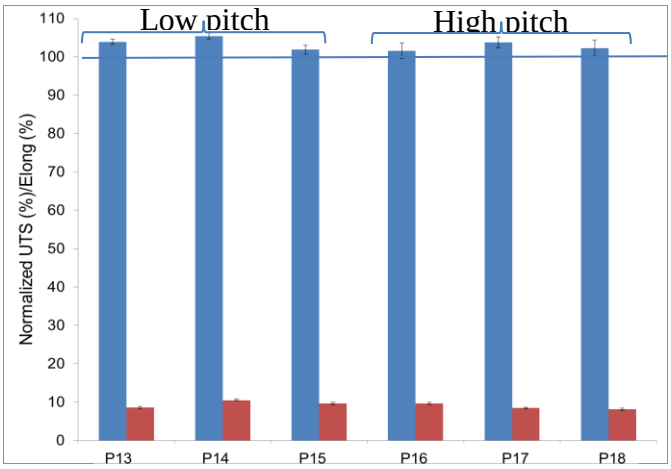

Figure 2. Summary of mechanical properties of the 0.95 cm thick SR-FSW panels tested RT.

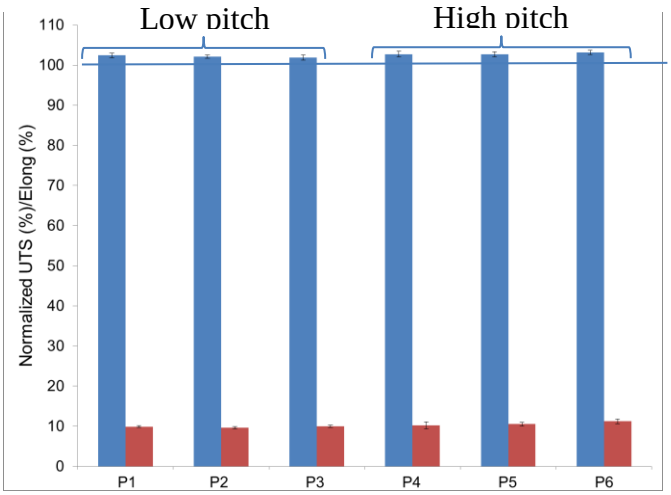

Figure 3. Summary of mechanical properties of the 1.27 cm thick SR-FSW panels tested at RT.

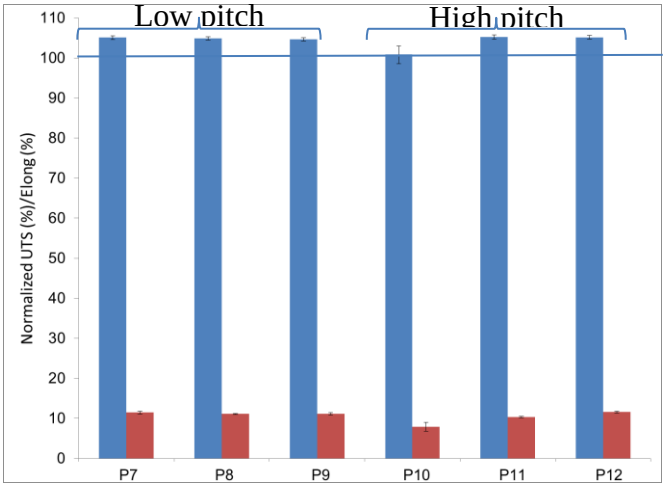

Figure 4. Summary of mechanical properties of the 1.59 cm thick SR-FSW panels tested at RT.

Table II. Selected specimens for metallographic inspection.

Specimen ID	Weld pitch (rev/in)	Individual UTS (normalized %)	Panel Average and Standard Deviation for UTS (normalized %)	Individual Elongation (%)	Panel Average and Standard Deviation for Elongation (%)	Fracture location
375-14-RT-1	Low	112.6	105.3 ± 0.8	10.7	10.5 ± 0.2	RS
375-17-RT-5	High	111.9	103.6 ± 1.5	8.8	8.5 ± 0.2	AS
375-18-RT-4	High	107.2	102.2 ± 2.0	7.7	8.1 ± 0.3	AS
375-15-M-03	Low	NA	101.8 ± 0.1	NA	9.6 ± 0.4	RS
500-02-RT-5	Low	101.7	102.0 ± 0.4	10.0	9.6 ± 0.2	RS
500-06-RT-2	High	103.0	103.0 ± 0.5	11.6	11.2 ± 0.6	AS
500-03-RT-2	Low	101.8	101.8 ± 0.7	9.7	10.0 ± 0.3	RS
500-05-RT-4	High	101.4	102.5 ± 0.6	9.9	10.5 ± 0.5	AS
625-07-RT-6	Low	104.6	105.1 ± 0.5	11.6	11.5 ± 0.4	RS
625-10-RT-3	High	100.3	100.8 ± 2.2	7.7	7.9 ± 1.1	AS

4.2 Metallographic studies

Representative images from specimens highlighted in Table II are shown in this section to document the macrostructure of "out of family values" for the normalized ultimate tensile strength (UTS) and elongation to failure. Figure 5 is a macrograph of a nominal strength weld using the lower weld pitch parameters which failed on the RS. Noted was a crack which extended through the nugget region. In comparison, Figure 6 shows a nominal strength weld joined at the higher weld pitch which failed on the AS. While the mechanical properties are within the acceptance criteria and little scatter is noted, the fractures are not considered to be typical of a robust FSW.

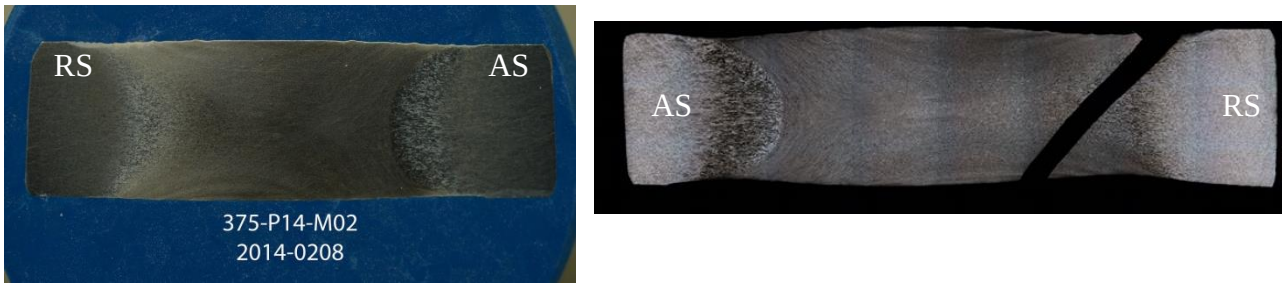

(a) (b)

Figure 5. (a) Metallograph for the M02 specimen in panel #375-14 and (b) the corresponding break observed for RT tensile specimen RT 1

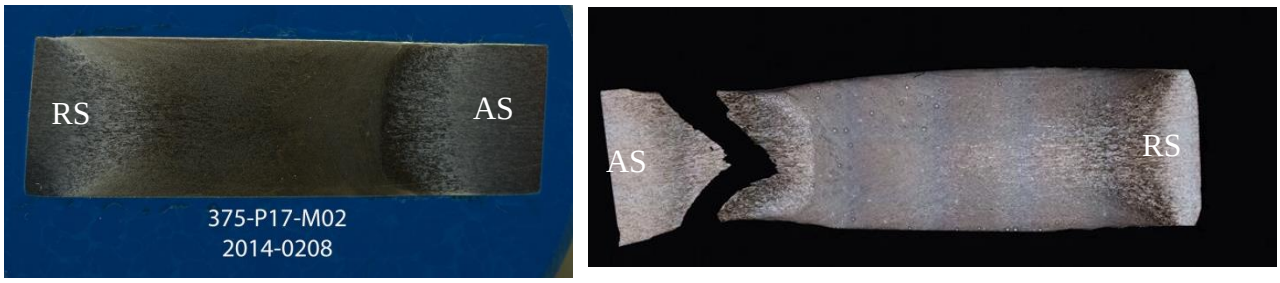

(a) (b)

Figure 6. (a) Metallograph for the M02 specimen in panel #375-17 and (b) the corresponding break observed in RT tensile specimen RT 5.

Figure 7 shows the metallograph for the lowest strength specimen joined at the low weld pitch which also fractured along the AS. Figure 8 shows some higher magnification images which capture the line feature in the nugget region. This line is not a crack as shown by Figure 8b, but shows the contrast originates from abnormally small grains and thickened grain boundaries.

This line feature was fairly common in all the 0.95 cm thick SR-FSWs as evidenced by Figure 9, which was also joined at the higher weld pitch. The appearance of these lines in the 0.95 cm thick SR-FSWs did not correlate with lower strength or ductility

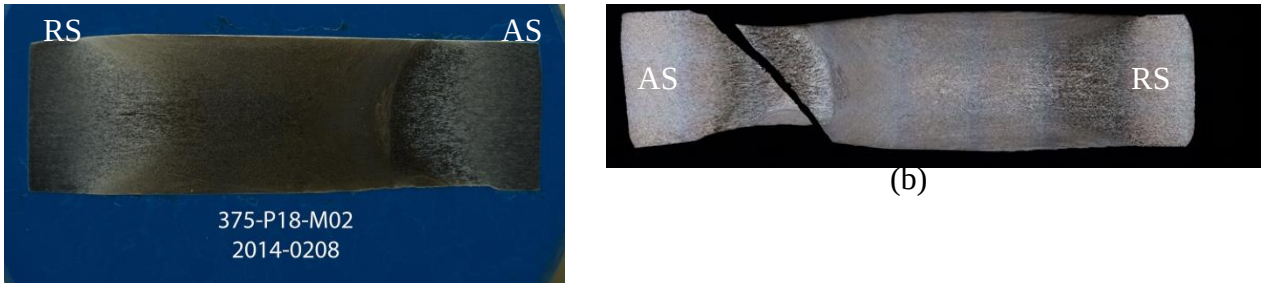

(b)

(a)

Figure 7. (a) Metallograph for the M02 specimen in panel #375-18, (b) corresponding RT break in tensile specimen RT-4.

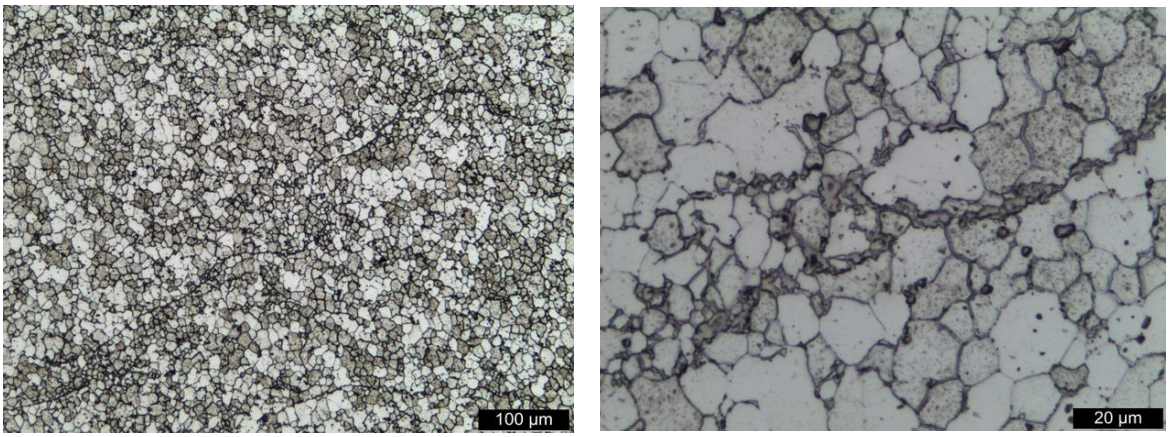

Figure 8. (a) Close up of line feature in SR-FSW #375-18-M01 and (b) associated fine grain region.

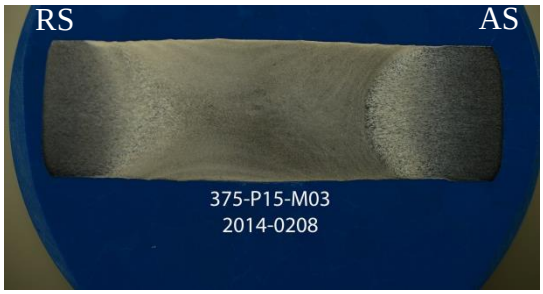

(a)

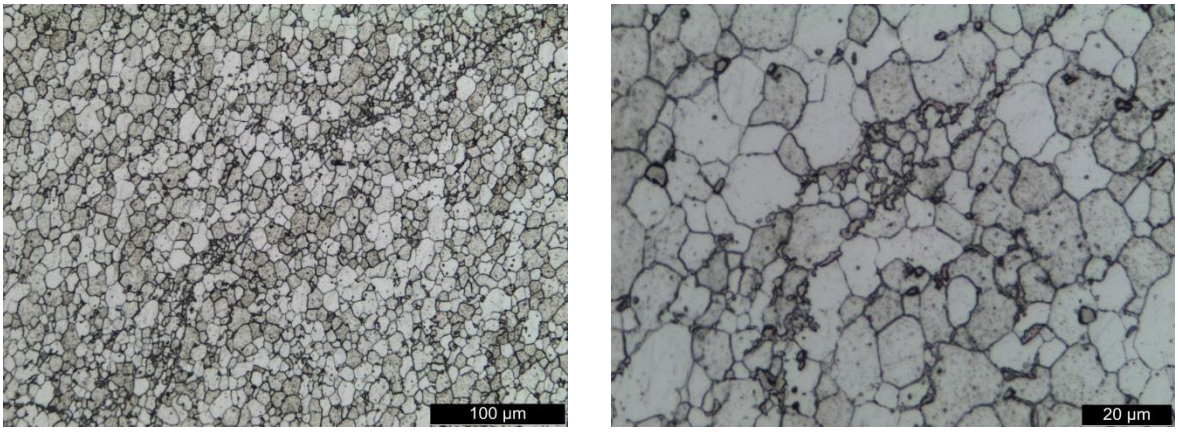

(b) (c)

Figure 9. (a) Metallograph for the M03 specimen in panel #375-15, (b) close up of line feature, and (c) associated grain details of line feature.

Similar characteristics were observed in the high and low property specimens for the 1.27 cm thick SR-FSW as shown in Figure 10 and 11. Further metallurgical examination of the low property weld is shown in Figure 12 which also shows the presence of the line feature.

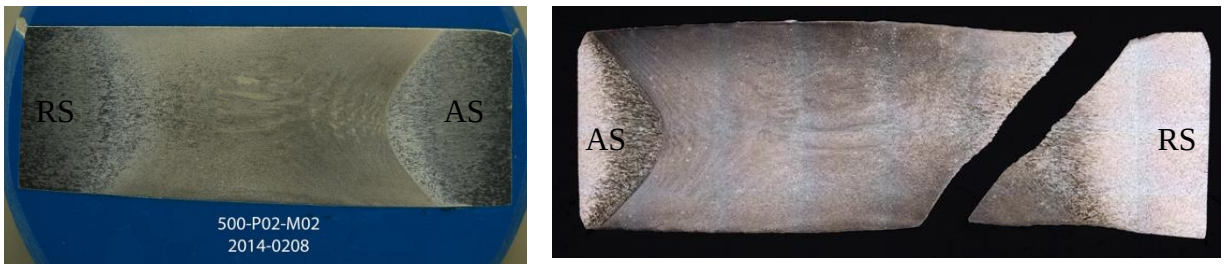

(a) (b)

Figure 10. (a) Metallograph for the M02 specimen in panel #500-02 and (b) corresponding fracture location in tensile specimen RT-5.

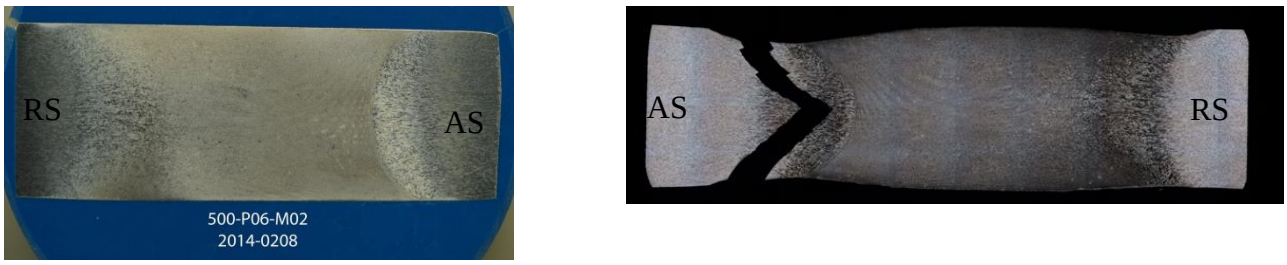

(a) (b)

Figure 11. (a) Metallograph for the M02 specimen in panel #500-P06 and (b) corresponding fracture location in tensile specimen RT-2.

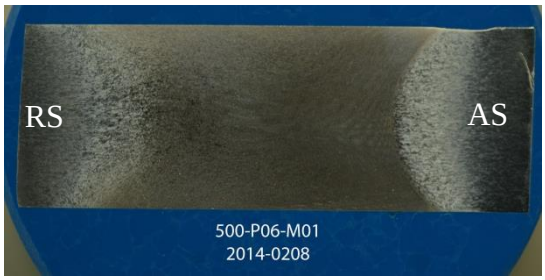

(a)

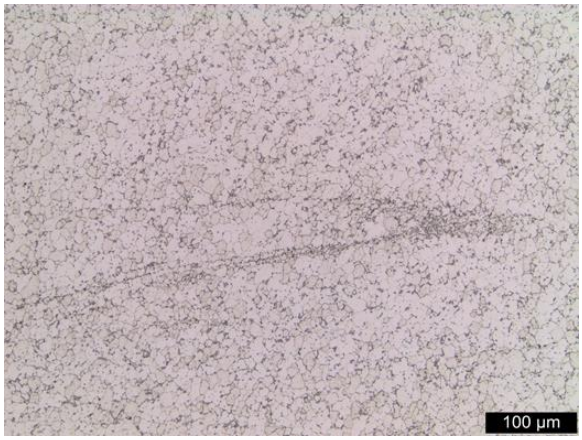

(b)

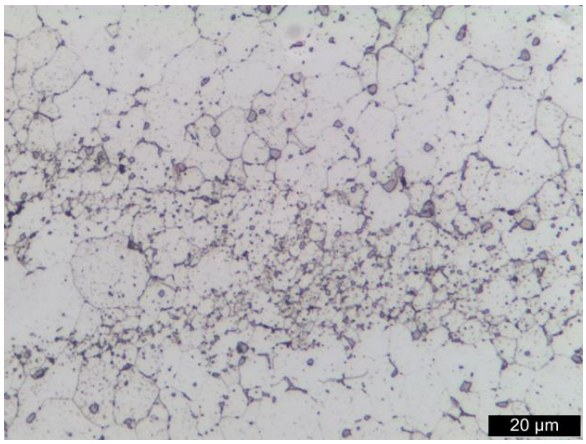

(c)

Figure 12. (a) Metallograph for the M01 specimen in panel #500-P06, (b) close-up of line feature in weld nugget, and (c) small grain region associated with the line feature.

The largest mechanical property variation was observed in the 1.59 cm thick SR-FSWs. Figure 13 shows a nominal property specimen which failed on the desired RS. The line indications were also observed within this weld nugget as shown in Figure 14. A close-up of this region in Figure 14b shows a region of very fine grains which give rise to this dark line appearance in Figure 14a.

Figure 13. Fracture location in specimen #625-P07-RT6 [33].

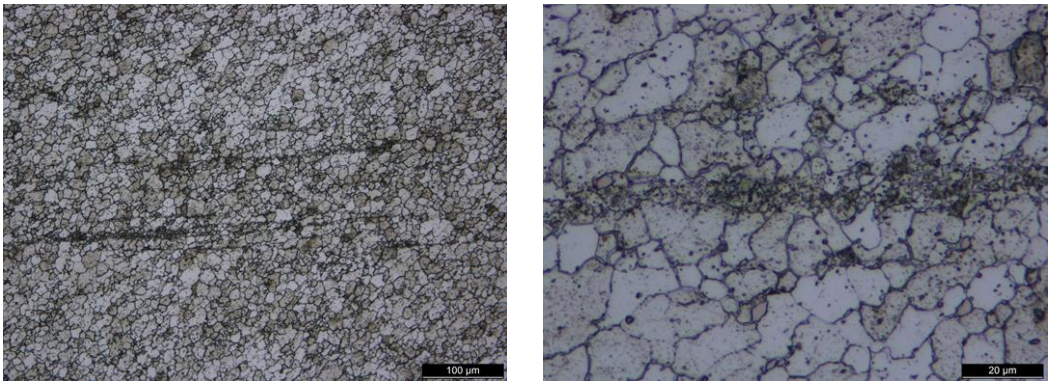

(a) (b)

Figure 14. (a) close-up of line feature in SR-FSW #625-P07-RT6 [33] and (b) associated fine grain features.

Figure 15 is a macrograph of the lowest strength SR-FSW in the 1.59 cm panels. The fracture path is on the AS and extends through the weld nugget, but in a more irregular and jagged pattern. Also noted within Figure 15 is evidence of tears on the AS root surface.
Figure 16 shows a series of images from the nugget of P10 SR-FSW which show the line feature observed in the other panel thickness. But these images also capture regions where tears have formed. Figure 17 shows one of these hot tears and also shows evidence of porosity in the region adjacent to the tear.

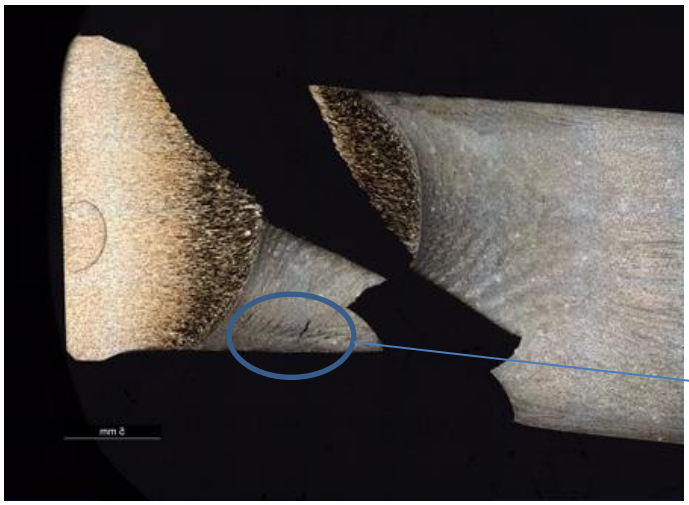

Figure 15. Fracture location for SR-FSW #625-P10-RT3 [33].

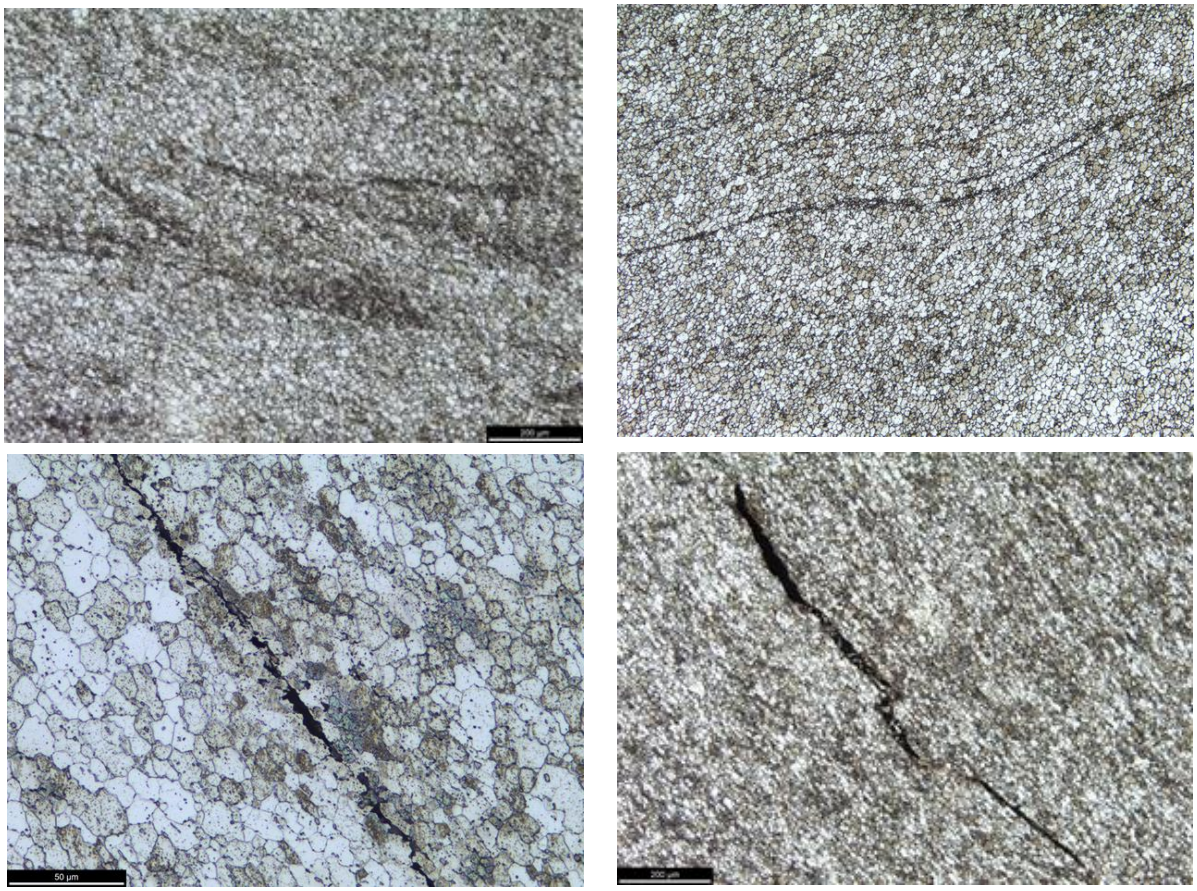

Figure 16. SR-FSW panel #625-P10-RT3 showing close up of regions with line features and the presence of hot tears [33].

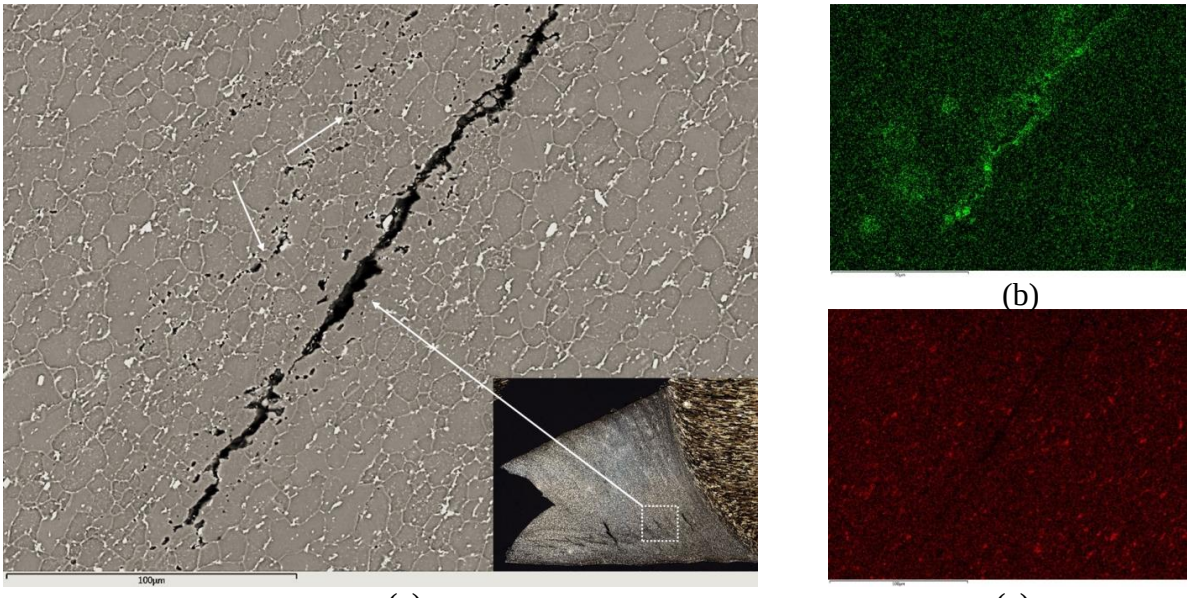

(a) (b) (c)

Figure 17. (a) Close up of hot tear in #625-P10-RT3 [33] and noted porosity in adjacent regions along with EDS maps for (b) oxygen and (c) copper.

5.0 Discussion

The tensile data shows some minor variation within the strength and elongation to failure. Although all values were within acceptable ranges, there were outliers, or out of family values, for several test specimens. Outliers suggest that something is occurring within the weld specimens that may appear somewhat random in occurrence but could compromise the robustness of the process if not understood and mitigated.

Although not all specimens broke on the RS of the weld nugget, there was no correlation of tensile break with the tensile results. Line features were observed in all SR-FSWs, but did not appear to be kissing type bonds or associated with remnant joint defects. Microstructural analysis of the weld zone showed an increasing tendency for regions of oxides associated with refined grains as the weld panel thickness increased to 1.59 cm. Additionally, in the 1.27 cm thick weld panels, tears were observed in these oxide rich, refined grain regions.

The temperature of the weld panel has been most strongly correlated with the tool rotation. The amount of torque required to form a FSW is related to temperature with higher temperatures reducing the torque. Considering these relationships, the 5% increase in weld pitch for the 0.95 cm thick panel did not appreciably change the temperature as the measured torque remains fairly constant. In contrast, increasing the weld pitch over 10% does correspond to a decrease in torque for both the 1.27 and 1.59 cm thick workpieces.

An observation, illustrated by Figure 18, is that as the weld panel increase in thickness there is an increasing gap ahead of the weld tool. A gap in advance of the weld tool can form as the force differential between the pin/root shoulder force and the crown shoulder force results in a load on the panels at the location of the joint. As the clamps are approximately 3.18 cm from the weld seam, the AS and RS side of the weld seam can be considered as a cantilever beam illustrated in Figure 19. The deflection of the cantilever beam assembly is given by y in equation 1 and the angle of deflection given by θ in equation 2. The resulting load (P) on the workpiece is the pinch force, or delta between the applied crown shoulder force and the pin/root shoulder force, and L is the distance from the weld seam to the clamp. E = 69 GPa, the elastic modulus of aluminum.

Figure 18. Root side image of the gap in a 3.18 cm thickness weld panel in advance of the weld tool at the end of the weld.

$$y = -\frac{P\,L^3}{3\,E\,I} \qquad \text{[eqn. 1]}$$

Where I is the moment of inertia given in equation 2, height (h) is the panel thickness, and the base (b) is assumed to be a unit of 1.

$$I = \frac{1}{12} b h^3 \qquad \text{[eqn. 2]}$$

The corresponding angle formed as the beam deflects is illustrated in Figure 19 and given as θ in equation 3.

$$\theta = \frac{P L^2}{2 E I} \qquad \text{[eqn. 3]}$$

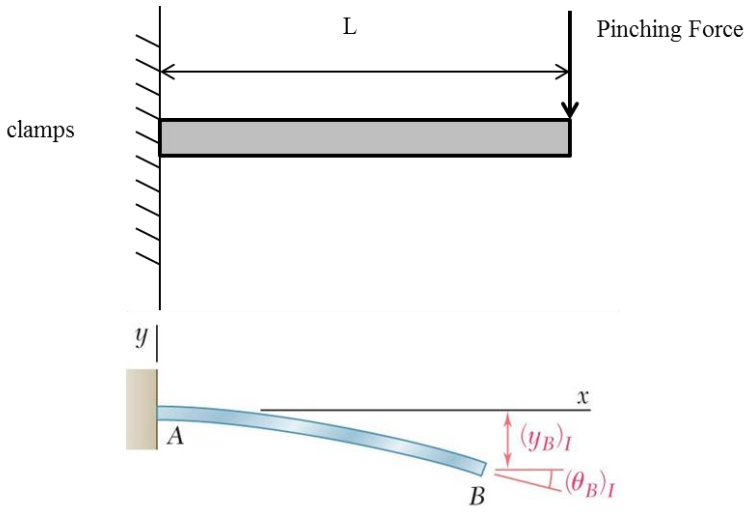

Figure 19. Beam deflection expected from resulting pinching force applied at weld seam.

Estimations of the deflection and angle are summarized in Table III. Although the increasing thickness of the workpiece increases the resistance to deformation, the deflection increases.

Table III. Calculated beam deflection.

load (P) (kN)	length (L) (cm)	thickness (cm)	deflection (y) (cm)	θ (degrees)
0.9	3.18	0.950	-0.246	2.09
2.2	3.18	1.270	-0.259	2.20
2.2	3.18	1.590	-0.132	1.13

Aluminum and its alloys are known to form a protective oxide coating. This oxide formation is almost instantaneous and follows a parabolic rate until an equilibrium thickness is formed. Although the rate of oxidization is influenced by temperature, moisture and alloying composition, it is in all cases self-limiting unless fractured. This oxide is not readily removed and requires fracturing either through the application of mechanical abrasives or shearing loads.

As the oxidation rate is noted to increase with increasing temperature, it is conceivable that the faying surface would be prone to increased oxidation during the FSW if exposed to entrained air. At the estimated FSW temperature of aluminum alloys (530 to 580 ºC), the oxidation behavior rate changes from parabolic to linear.

It is generally assumed that minimal entrained air enters the faying surface during a butt weld. However as the weld panels increase in thickness, it has been observed that gaps open in advance of the weld tool. As this gap increases, it can provide a passage way for air to enter causing enhanced oxidation at the elevated temperatures as illustrated in Figure 20. This would be further exasperated if second phases or precipitates were to liquate at the welding temperature. Exposure to air at these temperatures would oxidize these molten regions which would tend to be located at the grain boundaries.

Figure 20 illustrates sealing up and oxidation of a weld seam as it follows a streamline around a FSW pin shown in a plan view. In Figure 20 the gap closure distance illustrated is on the order of the shear surface thickness, a few thousandths of a cm. In actuality, although the gap closure configuration doubtless plays a significant role in determining the state of oxidation of the seam residue, it has not been studied as far as the authors of this work are aware. In addition the gap width can also be altered by the weld parameters.

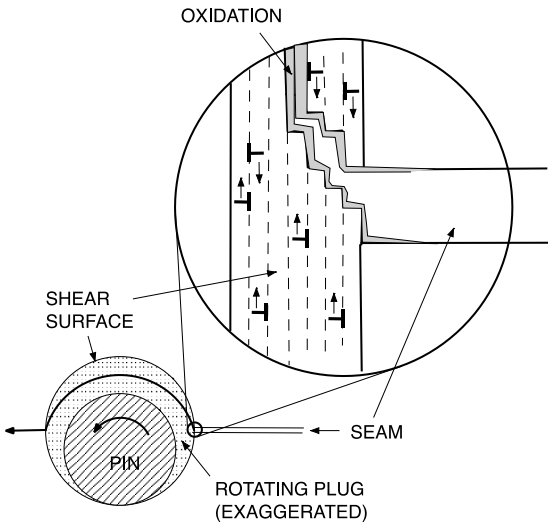

Figure 20. Schematic of a plan view of the FSW zone in which the weld seam is shown entering the shear surface (slip line) in which bounding metal clings to the FSW pin as a streamline. The material travels from right to left while the tool rotates in a counter-clockwise direction. The seam acquires surface oxide before it is sealed up, or welded. A hypothetical surface oxidation within the shear "surface", actually a thin extended region, is shown. The seam continues along its streamline to emerge behind the tool as a welded seam remnant incorporating oxide.

If oxygen is entrained with air introduced within the gap opening, its rate would also be expected to be effected by diffusion within this region. The rate of oxidation would compete between the oxygen diffusion to the metal vs the depletion of oxygen from the gap. Thus this occurrence could also depend on time at temperature as affected by the process parameters of weld pitch.

The chemical composition will also affect the resulting 2^{nd} phases present in the panels. Cu content can vary especially in AA2219. With higher Cu concentrations, there would be more excess θ phase which could explain variation among different lots of AA2219. Similar concerns would be expected with variations in both Cu and Li content in the 2195/2099 series of alloys.

6.0 Summary

Studies in the literature on the "lazy Z" have concluded that non-optimized parameters are responsible for the reduction observed in mechanical properties. Thus the seemingly random occurrence of oxides in FSWs suggests there is an underlying cause. This study considers another mechanism of oxidation within a FSW nugget. Since thicker oxides require higher temperatures, in excess of 500 ºC, to form this could be promoted on the interior surfaces during a FSW if exposed to entrained air.

Understanding this cause and effect would improve the robustness of the process. Possible causes include:

1) Variations in amount of alloying elements in the workpiece.
2) Higher temperatures during FSWs may promote oxidation on internal surfaces.
3) Gap separation of thicker panels in advance of the FSW tool may provide a pathway for entrained air during the FSW process.

Thus incorporation of a purge gas during SR-FSW process may be needed to mitigate oxide formation, especially in thicker workpieces. Correlation of pinch force in SR-FSWs should help to identify the air entrainment path from either the crown or root side.

7.0 References

1) P.E. Doherty, R.S. Davis, "Direct Observation of the Oxidation of Aluminum Single-Crystal Surfaces," J. Appl. Phys., vol. 34, pp. 619-628, 1963.
2) K. Thomas, M.W. Roberts, "Direct Observation in the Electron Microscope of Oxide Layers on Aluminum," J. Appl. Phys., vol. 32, pp. 70-75, 1961.
3) A. Steinheil, Ann. Phys., "Struktur und wachstum duenner obserflaechenschiechten auf metallen bei oxydation an luft," vol. 19, no. 5, pp. 465-483, 1934.
4) M.A. Trunox, M. Schoenitz, X. Zhu, E.L. Dreizin, "Effect of polymorphic phase transformations in Al_2O_3 film on oxidation kinetics of aluminum powders," Combustion & Flame, vol. 140, pp. 310-318, 2005.

5) J.C. Sanchez-Lopez, A.R. Gonzalez-Elipe, A. Fernandez, "Passivation of nanocrystalline Al prepared by the gas phase condensation method: an XPS study," J. Mater. Res., vol. 13, no. 3, pp. 703-710, 1998.
6) R.K. Hart, "The oxidation of aluminum in dry and humid oxygen atmospheres," Proceed. Royal Society of London, Series A. Mathematics & Physical Sciences, vol. 236, no. 1204, pp. 68-88, 1956.
7) W.W. Smeltzer, "Oxidation of Aluminum in the Temperature Range of 400º to 600º C," J. Electrochemical Soc., pp. 209-214, April 1956.
8) L. P. H. Jeurgens, W. G. Sloof, F. D. Tichelaar, and E. J. Mittemeijerc, "Growth kinetics and mechanisms of aluminum-oxide films formed by thermal oxidation of aluminum," J. Appl. Phys., vol. 92, pp. 1649, 2002.
9) E. Bergsmark, C.J. Simenen, P. Kofstad, "The oxidation of molten aluminum," MSEA, vol. 120, pp. 91-95, 1989.
10) W. Thiele, Aluminum, vol. 38, pp. 707-786, 1962.
11) C.N. Cochran, D.L. Belitskus, D.L. Kinosz, "Oxidation of aluminum-magnesium melts in air, oxygen, flue gas, and carbon dioxide," Metall. Trans. B, vol. 8, pp. 323-332, 1977.
12) Y-J. Oh, J-I. Mun, J-H. Kim, "Effects of alloying elements on microstructure and protective properties of Al_20_3 coatings formed on aluminum alloy substrates by plasma electrolysis," Surface & Coatings Technology, vol. 204, pp. 141-148, 2009.
13) J.H. Record, J. L. Covington, T.W. Nelson, C.D. Sorensen, B.W. Webb, "A look at statistical identification of critical process parameters in friction stir welding," Welding Journal, vol. 86, no. 4, pp. 97s - 103s, 2007.
14) J.A. Schneider, R. Stromberg, P. Schilling, B. Cao, W. Zhou, J. Morfa, O. Myers, "Processing effects on the friction stir weld stir zone," Welding Journal, pp. 11s-19s, January 2013.
15) B. Li, Y. Shen, W. Hu, "The study on defects in aluminum 2219-T6 thick butt friction stir welds with the application of multiple non-destructive testing methods," Materials and Design, Vol. 32, pg. 2073–2084, 2011.
16) H-B. Chen, K. Yan, T. Lin, S-B. Chen, C-Y. Jiang, Y. Zhao., "The investigation of typical welding defects for 5456 aluminum alloy friction stir welds," MSEA Vol. 433, pg. 64–69, 2006.
17) H. K. Klages, "The "Lazy S" feature in friction stir welding of AA2099 Aluminum-Lithium alloy," Navy Postgraduate School, Monterey, CA, MS Thesis, December 2007.
18) A.J. Leonard, S.A. Lockyer, "Flaws in friction stir welds," 4th Intl. Symp. FSWing, Park City, Utah, May 14-16, 2003.
19) H.J. Liu, Y.C. Chen, J.C. Feng, "Effect of zigzag line on the mechanical properties of friction stir welded joints of an Al–Cu alloy," Scripta Mat., Vol 55, pp. 231-234, 2006.
20) Private conversation with Murray Mahoney, formerly of Rocketdyne, January 2016.
21) A. C. Nunes, Jr. "Metal Flow in Friction Stir Welding," Conf. Proc., MS&T, 2006.
22) D.P. Field, T.W. Nelson, Y. Hovanski, K.V. Jata, "Heterogeneity of Crystallographic Texture in Friction Stir Welds of Aluminum," Metall. Mater. Trans. A, vol. 32, pp. 2869-2877, 2001.
23) Y.S. Sato, H. Kokawa, K. Ikeda, M. Enomoto, S. Jogan, T. Hasimoto, "Microtexture in the friction stir weld of an aluminum alloy," Metall Mater Trans A, vol. 32, pp. 941-948, 2001.

24) S.H.C. Park, Y.S. Sato, H. Kokawa, "Microstructural factors governing hardness in friction-stir welds of solid-solution-hardened Al alloys," Metall. Mater. Trans A, vol. 32, no. 12, pp. 3033-3042, 2001.
25) Y.S. Sato, F. Yamashita, Y. Sugiura, S.H.C Park, H. Kokawa, "FIB-assisted TEM study of an oxide array in the root of a friction stir welded aluminum alloy," Scripta Mater., vol. 50, pp. 365–369, 2004.
26) K.N. Krishnan, "On the formation of onion rings in friction stir welds," Mater. Sci. Eng. A, vol. 327 pp. 246–251, 2002.
27) H. Larsson, et al., "Joining of dissimilar Al-alloys by Friction Stir Welding," 2nd Intl. Conf. Friction Stir Welds, Gothenburg, Sweden, 2000.
28) R. Crawford, G.E. Cook, A.M. Strauss, D.A. Hartman, M.A. Stremler, "Experimental defect analysis and force prediction simulation of high weld pitch friction stir welding," Sci Technol Weld Joining, vol. 11, pp. 657–665, 2006.
29) H.J. Liu, H, Fujii, M. Maeda, K. Nogi, "Tensile fracture location characterization of friction stir welded joints of different aluminum alloys," J. Mater. Sci. Technol., vol. 20, pp. 103–105, 2004.
30) X. Long, S.K. Khanna, "Modelling of electrically enhanced friction stir welding process using finite element method," Sci. Technol. Weld Joining, vol. 10, pp. 482–487, 2005.
31) Y.G. Kim, H, Fujii, T. Tsumura, T. Komazaki, K. Nakata, "Three defect types in friction stir welding of aluminum die casting alloy," Mater. Sci. Eng. A, vol. 415, pp. 250–254, 2006.
32) M. Fisher, Boeing Company Memo, #EYBF-MAF-14-029, October 16, 2014.
33) P-S. Chen, "Weld microstructure analysis for 2219-T8/2219/T8 SR FSW," Jacobs ESSSA Group/Qualis Corporation, Presentation to EM30/NASA MSFC, July 13, 2015.